Computers in Biology and Medicine 170 (2024) 108011

Contents lists available at ScienceDirect

Computers in Biology and Medicine

journal homepage: www.elsevier.com/locate/compbiomed

Cellular subpopulations identified using an ensemble average of multiple dielectrophoresis measurements

Seungyeop Choi [a,b,c,1], Sung-Hun Woo [d,1], Insu Park [e,f,1], Sena Lee [g], Kang In Yeo [a], Sang Hyun Lee [a], Sei Young Lee [a,n], Sejung Yang [g], Gyudo Lee [h,i], Woo-Jin Chang [j], Rashid Bashir [e,k,l,m], Yoon Suk Kim [d,**], Sang Woo Lee [a,*]

[a] Department of Biomedical Engineering, Yonsei University, Wonju, 26493, Republic of Korea
[b] School of Biomedical Engineering, Korea University, Seoul, 02481, Republic of Korea
[c] BK21 Four Institute of Precision Public Health, Korea University, Seoul, 02841, Republic of Korea
[d] Department of Biomedical Laboratory Science, Yonsei University, Wonju, 26493, Republic of Korea
[e] Holonyak Micro and Nanotechnology Laboratory, University of Illinois at Urbana-Champaign, Urbana, IL, 61801, USA
[f] Department of Biomedical Engineering, Konyang University, Daejeon, 35365, Republic of Korea
[g] Department of Precision Medicine, Wonju College of Medicine, Yonsei University, Wonju, 26426, Republic of Korea
[h] Department of Biotechnology and Bioinformatics, Korea University, Sejong, 30019, Republic of Korea
[i] Interdisciplinary Graduate Program for Artificial Intelligence Smart Convergence Technology, Korea University, Sejong, 30019, Republic of Korea
[j] Mechanical Engineering Department, University of Wisconsin-Milwaukee, Milwaukee, WI, 53211, USA
[k] Department of Mechanical Science and Engineering, University of Illinois at Urbana—Champaign, Urbana, IL, 61801, USA
[l] Department of Bioengineering, University of Illinois at Urbana—Champaign, Urbana, IL, 61801, USA
[m] Materials Research Laboratory, University of Illinois at Urbana—Champaign, Urbana, IL, 61801, USA
[n] Department of Medical Informatics and Biostatistics, Graduate School, Yonsei University, Wonju, 26426, Republic of Korea

ARTICLE INFO

Keywords:
Dielectrophoresis
DEP crossover frequency
Ensemble average
Multiple measurements
Subpopulation discrimination

ABSTRACT

While the average value measurement approach can successfully analyze and predict the general behavior and biophysical properties of an isogenic cell population, it fails when significant differences among individual cells are generated in the population by intracellular changes such as the cell cycle, or different cellular responses to certain stimuli. Detecting such single-cell differences in a cell population has remained elusive. Here, we describe an easy-to-implement and generalizable platform that measures the dielectrophoretic cross-over frequency of individual cells by decreasing measurement noise with a stochastic method and computing ensemble average statistics. This platform enables multiple, real-time, label-free detection of individual cells with significant dielectric variations over time within an isogenic cell population. Using a stochastic method in combination with the platform, we distinguished cell subpopulations from a mixture of drug-untreated and -treated isogenic cells. Furthermore, we demonstrate that our platform can identify drug-treated isogenic cells with different recovery rates.

1. Introduction

Most cellular research measures average values among cells in a population to successfully analyze and predict the general behaviors and properties of that population [1]. However, that approach sometimes fails, particularly when significant differences occur among individual cells within a single isogenic cell population. Such significant differences among individual cells can originate from intracellular changes such as differences in cell cycles, different cellular responses to certain stimuli, or even uncontrolled microenvironments around cells, and they make it challenging to explain the behaviors and properties of a cell population using only average values [1–4]. Cellular diversity that originates from intrinsic changes in individual cells can create subpopulations in an isogenic cell population. For example, individual cancer cells in an

* Corresponding author.
** Corresponding author.
E-mail addresses: yoonsukkim@yonsei.ac.kr (Y.S. Kim), yusuklee@yonsei.ac.kr (S.W. Lee).
[1] These authors contributed equally to this work.

https://doi.org/10.1016/j.compbiomed.2024.108011
Received 8 October 2023; Received in revised form 11 January 2024; Accepted 16 January 2024
Available online 18 January 2024

isogenic population can respond differently anticancer drugs. Non-genetic adaptation to an anticancer drug can make an initially homogenous drug-treated cancer cell population heterogeneous, allowing subpopulations to emerge [5,6]. As another example of subpopulation growth in an isogenic cell population as a result of different responses to the surrounding microenvironment, cancer cells able to undergo metastasis or immune evasion can appear in an isogenic tumor cell population that is initially incapable of either behavior [7].

Therefore, analyzing cellular properties and behaviors at the subpopulation level, rather than the whole population level, would be a better way to examine cellular responses to certain external stimuli. Distinguishing subpopulations within an isogenic cell population requires that the biological noise and systemic measurement noise generated during measurement procedures be minimized to ensure the generation of statistically reliable data. In general, experiments are repeated at the macro-scale level to reduce such noise and improve the precision of the values measured in various cell experiments. However, it is difficult to simultaneously observe individual cell behaviors in the exact same microenvironmental conditions, which is essentially for the study of subpopulations within an isogenic cell population, in repeated macro-scale experiments.

In recent years, micro/nano-techniques for examining cellular characteristics inside a microfluidic device have advanced rapidly. These techniques can simultaneously probe the behaviors of individual cells in the same environmental conditions, producing the reliable and robust data needed to investigate the biophysical properties of cells. Optical [8], dielectrophoretic [9–11], magnetic [12], acoustic [13,14], and hydrodynamic [15] techniques are examples of such methods. These manipulation techniques take advantage of the gradient force in an external field, which induces particle motion based on force differences at the particle interface in response to the external field. Initially, they were mainly used to improve the efficiency of conventional molecular biomarker-based biochemical analysis as a single-cell trapping and separation techniques [8,9,12–16]. More recently, their importance has grown as various biophysical characteristics have been shown to serve as an additional phenotypic biomarker for distinguishing cell heterogeneity at the cellular level [17]. Biophysical biomarkers such as cell morphology (including size and membrane roughness), cell mass, stiffness, mean square displacement, deformability, and cytoplasmic conductivity have been identified. Using both/either biochemical and/or biophysical biomarkers, these micro/nano techniques have been successfully applied to discriminate cell heterogeneity between different types of stem cells, white blood cells, red blood cells, and cancer cell populations [18–29]. Among them, the dielectrophoretic (DEP) technique, in which a single cell is placed on an isolated trap inside a microfluidic device, has come into the spotlight because it is label free and can manipulate and investigate the dielectric properties of numerous individual cells at once [30,31]. Probing cancer cells in a mixture sample with normal cells and blood cells [32], differentiating cell lineages [33,34], and detecting leukocyte activation [35] are excellent examples of manipulating numerous individual cells while investigating each cell's dielectric properties.

Therefore, the DEP technique seems to provide a great opportunity to detect and distinguish cell subpopulations within an isogenic cell population. However, DEP-based measurement techniques produce a snapshot observation of each cell's DEP behavior at a discrete time; they do not track the DEP behaviors of numerous individual cells over time [30,36]. Therefore, we recently developed a DEP-based method for tracking numerous individual cells simultaneously and performing multiple measurements of each cell's DEP behavior over time [37]. This method is very promising for distinguishing and characterizing subpopulations in an isogenic cell population because the developed DEP techniques can obtain more reliable data than previous methods while tracking numerous individual cells through time.

In this study, we report a stochastic approach that uses an ensemble average of multiple measurements obtained using our new DEP technique to distinguish cellular subpopulations that originate from an isogenic cell population. To verify the stochastic approach, we first examined whether our platform can distinguish two different subpopulations (untreated and methyl-β-cyclodextrin (MβCD)-treated MCF-7 cells) mixed in a population. The model mixture of untreated and MβCD-treated MCF-7 cells was discriminated using the ensemble average based on the less than 5 % overlap of two distributions, which was calculated from multiple measurements of individual cells' DEP cross-over frequencies. Furthermore, we differentiated subpopulations formed during the recovery of cellular changes generated by exposure to MβCD. Those results indicate that our stochastic approach using the ensemble average of multiple measurements can discriminate cell subpopulations from a mixture in real-time without further isolation of the subpopulations.

2. Materials and Methods

2.1. Materials and reagents

Dulbecco's modified Eagle's medium (DMEM), fetal bovine serum (FBS), penicillin-streptomycin, 0.25 % trypsin-EDTA, and phosphate-buffered saline (PBS; × 1) were purchased from Gibco (Gaithersburg, MD, USA). D-glucose and sucrose were purchased from Bio Basic Inc. (Markham, ON, Canada). Bovine serum albumin (BSA) was purchased from Bovogen Biologicals (Essendon, VIC, Australia). Plasmocin Prophylactic (0.2 %) was purchased from InvivoGen (San Diego, CA, USA). MβCD powder was purchased from Sigma-Aldrich (St. Louis, MO, USA). Deionized water was supplied by a purification system from Sartorius AG (Gottingen, Germany). Silicon dioxide wafers were purchased from *i*-Nexus (Seongnam, Republic of Korea), and polydimethylsiloxane (PDMS, Sylgard 184) agents and silicone elastomer curing agent were purchased from Dow Corning (Midland, MI, USA). Cover glasses were purchased from Marienfeld (Lauda-Königshofen, Germany).

2.2. Cell preparation

MCF-7 human breast cancer cells (ATCC, Manassas, VA, USA) were incubated in DMEM supplemented with 10 % FBS, 1 % penicillin-streptomycin, and 0.2 % Plasmocin Prophylactic at 37 °C in a humidified atmosphere with 5 % CO_2. For the DEP experiments, MCF-7 cells were seeded into six-well plates at 2×10^5 cells/well in the same buffer solution and cultivated for 48 h. After that, the cells were incubated in serum-free DMEM buffer with/without MβCD agents using the conditions described below. Then the cells were harvested using 0.25 % trypsin/EDTA solution and exchanged into DEP buffer solution containing 8.6 % (w/w) sucrose, 0.3 % (w/w) D-glucose, 0.20 % (v/v) PBS buffer, and 1.0 mg/mL BSA.

2.3. MβCD treatment conditions

We prepared a stock solution of 37.87 mM C4555 MβCD in a distilled water, divided it into small aliquots, and stored them at 4 °C before the DEP experiments. Next, we diluted the stock solution with serum-free DMEM buffer to a 10 mM solution of MβCD. This MβCD solution was administered to MCF-7 cells on a plate for 2 h and then exchanged with fresh serum-free DMEM buffer. After that, the treated cells were trypsinized for the DEP experiment. In the recovery experiment, the serum-free DMEM buffer containing MβCD was removed after 2 h of MβCD treatment, and fresh serum-free DMEM buffer without MβCD was added in a culture dish. After a 24-h incubation, the cells were trypsinized as in the DEP experiment.

2.4. DEP chip preparation

For the DEP-based cell assay, we fabricate microfluidic microelectrode array chips as shown in Fig. 1A, each composed of a DEP electrode

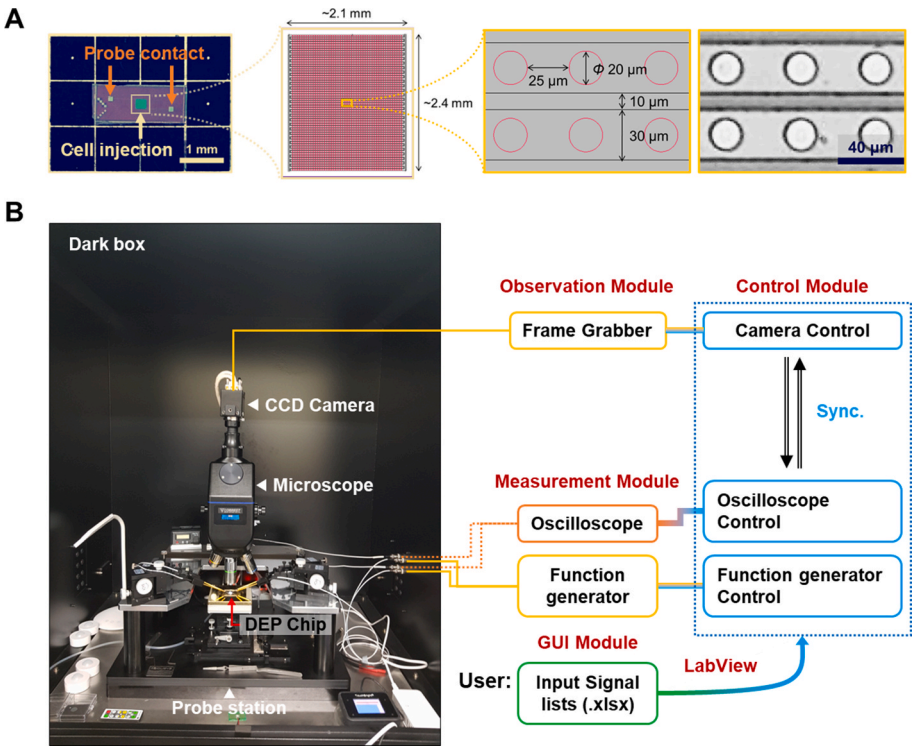

Fig. 1. Setup of the operation system for the proposed DEP platform. (**A**) The photograph of the fabricated chip consisting of 30 pairs of interdigitated electrode array and two contact electrode pads. (**B**) The electrical signals are applied to the contact pad through a micromanipulator connected to a 1 μm-diameter tungsten probe tip.

and a microfluidic chamber. Briefly, the DEP electrode was designed and fabricated in a 30-pair of interdigitated electrode array (30-μm wide chromium electrode fingers with 10-μm spacing and 0.1-μm thickness) on a silicon dioxide wafer, and then an insulator layer (0.8 μm of silicon dioxide) was deposited using a standard microfabrication technique [9]. Subsequently, the contact pad portions and circular hole array of the electrode array were etched in optimized wet-etching conditions. To observe the behavior of living cells on the DEP electrode, a PDMS chamber with 6-μl capacity was put into contact with the DEP electrode surface. A more detailed procedure is provided in our previous report [11].

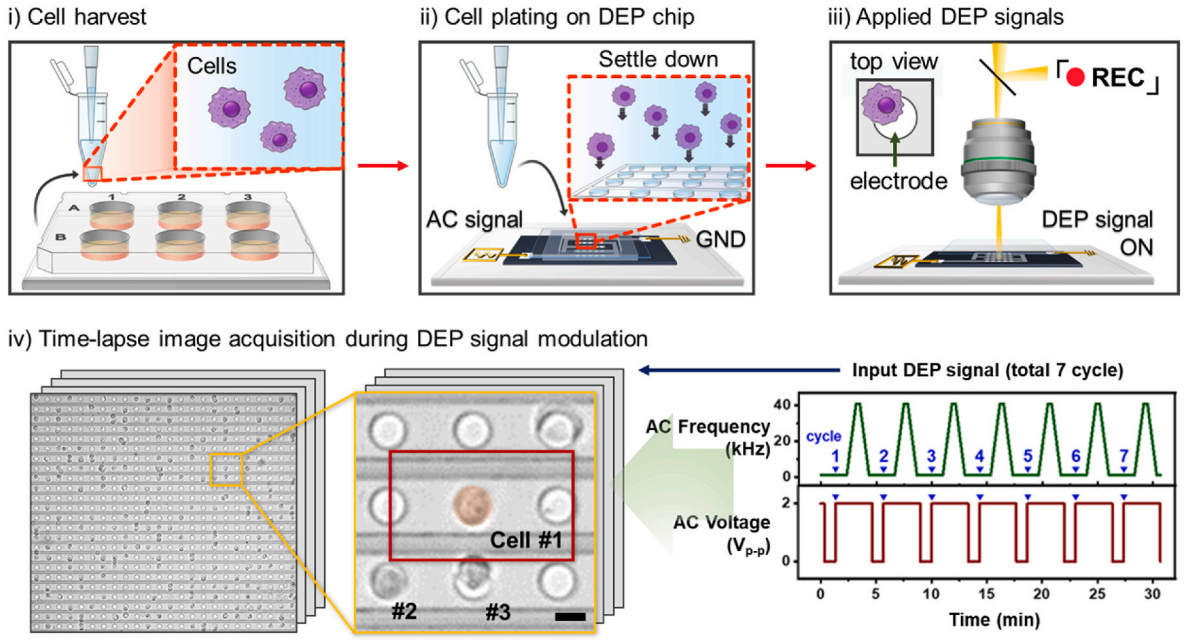

Fig. 2. Preparation process for the observation of DEP-induced cell mobility on our proposed platform. A detached cell sample is injected into the cleaned chip preparation for a DEP experiment (i-iv). The CCD camera recorded the DEP force-induced cell movement, which consists of the seven times repeated AC frequency and voltage change.

2.5. Platform operation

Our DEP signal modulation represents the variation of magnitude and direction of the DEP force controlled by AC frequency. The AC voltage is constant with 2 $V_{peak\text{-}peak}$ as the AC frequency changes (see lower-right inset of in Fig. 2). after the AC frequency is changed, the AC voltage was turned off for 1 min to minimize electrical cell damage. An AC signal was applied to two contact pads on the chip using a custom probe station (Modusystems, Inc., Hanam, Republic of Korea) that was connected to a modified automated DEP system. The system consisted of a control module, an observation module, and a signal generation module (Fig. 1B). The observation module consisted of a Wavesurfer 432 oscilloscope (Teledyne Lecroy Corp., Chestnut Ridge, NY, USA) and a Motionscope M3 digital camera (Redlake, San Diego, CA) and was connected to a PS-888 optical microscope (Seiwa Optical, Tokyo, Japan). The signal generation module consisted of an NI PCI-5421 PCI board (National Instrument, Austin, TX, USA). The control module ran LabVIEW software (National Instruments, Austin, TX, USA) to synchronize the signal generation and observation modules. The software controlled the input AC voltage and frequency (the lower-right inset of Fig. 2) through an arbitrary function generator. The input voltage amplitude and frequency were monitored by the oscilloscope. During modulation of the DEP signals, cell movements were recorded on a charge-coupled device camera that was connected to the control module. The detailed operation procedure is described in our previous report [38].

2.6. Data analysis

The DEP data (DEP cross-over frequency (f_{co}) and cell radius (r_{cell})) were analyzed using custom MATLAB codes to segment and track the cells of interest [37]. For all samples, the only cells we used as subjects were fully tracked during DEP signal modulation and trapped on the circular holes at the trapping frequency (AC 41 kHz). The acquired f_{co} data were sorted into three method groups (single, multiple, and average). The detailed data processing method is described in Materials and Methods 2.7 and Fig. 3. Cell radii were measured in the condition in which most cells were trapped by a constant DEP force at an identical input frequency. The DEP cross-over frequency was determined by estimating the border frequency between trapped and released cell mobility using the transition of DEP force [11]. The coefficient of variation (CV) for each dataset was calculated by dividing the standard deviation for the examined cells by the mean (i.e., CV = standard deviation of a population/mean of a population). Regarding our CV comparison calculation, we used a relative percentage procedure (e.g., $[CV_{multiple}\text{-}CV_{average}]/CV_{multiple} \times 100$ in comparison of CV with multiple and ensemble average method. We examined the Pearson correlation coefficient using Origin software to investigate the cell radius and DEP f_{co}. The Gaussian mixture model (GMM) method used to classify subpopulations was conducted using MATLAB library functions. In the drug recovery experiments, the optimum number of subpopulations was determined using Bayesian information criterion scores, bounded by 1–5 (see Fig. S5). Details related to our statistical analysis are provided in Supplementary Method S1.

2.7. Data processing for DEP-induced cell mobility measurement

We categorized DEP data from individual cells, which we obtained during the 7-cycle DEP signal modulation including AC Voltage and AC frequency, as shown in Fig. 2, to validate three measurement methods that all use the cell DEP properties of f_{co} and r_{cell}. First, we classified DEP data for a single cell via a MATLAB interface that uses a cell labeling procedure with an optimized single cell tracking analysis [37]. The data from single DEP measurements were selected in the first cycle of DEP signal modulation to reflect the procedure generally used in DEP experiments (light blue box in Fig. 3). Given that the total number of cells is *i cells*, and the total number of measurements is *N* cycles, we define the set of cell DEP data ($\{\chi_i\}$) involving f_{co} and r_{cell} as follows:

$$\{\chi_i\}_{Method} = \{\chi_1, \chi_2, \ldots, \chi_i\}_N \,|\{(f_{co})_i\} \in \{\chi_i\},\ \{(r_{cell})_i\} \in \{\chi_i\} \quad (1)$$

Because a single measurement occurs when *N* is 1, the dataset for single measurements ($\{\chi_i\}_{single}$) can be represented as follows:

$$\{\chi_i\}_{Single} = \{\chi_1, \chi_2, \ldots, \chi_i\}_{N\,=\,1} \quad (2)$$

All the DEP data obtained during seven signal modulation cycles were used for the multiple DEP measurement datasets (orange box in Fig. 3). Our experiments used 7 cycles (i.e., $N = 7$). Therefore, the multiple measurement dataset ($\{\chi_i\}_{multiple}$) can be represented as follows:

$$\{\chi_i\}_{Multiple} = \{\chi_1, \chi_2, \ldots, \chi_i\}_{N\,=\,1:7} \quad (3)$$

Finally, the sum of those values was averaged as an ensemble average using the seven cycles for each cell in each experimental condition (purple box in Fig. 3). The dataset for *i* cells calculated with the ensemble average method ($\{\chi_i\}_{Average}$) can be represented as follows:

$$\{\chi_i\}_{Average} = \left\{ \frac{\sum_{N=1}^{7} (\chi_1)_N}{7}, \frac{\sum_{N=1}^{7} (\chi_2)_N}{7}, \ldots, \frac{\sum_{N=1}^{7} (\chi_i)_N}{7} \right\} \quad (4)$$

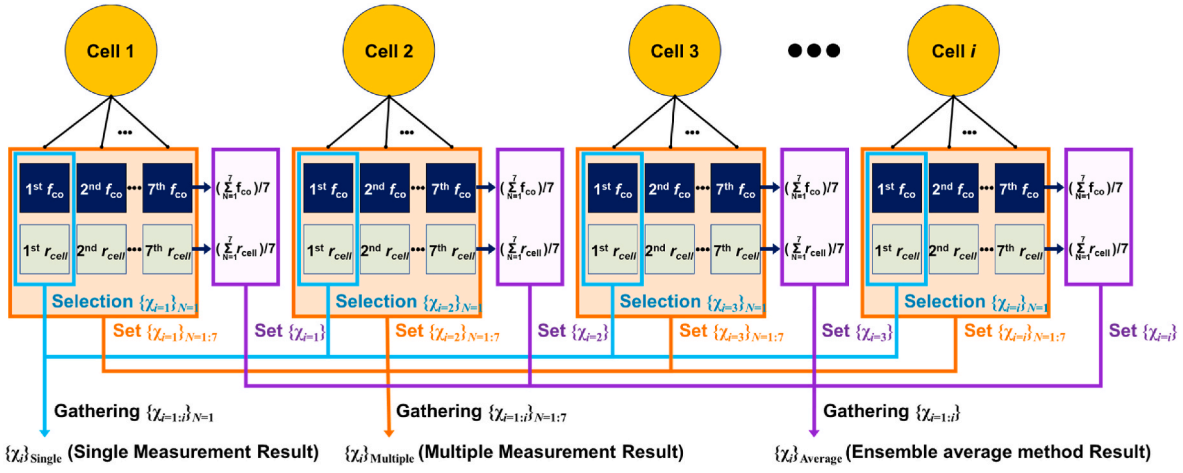

Fig. 3. Schematic presentation of the calculation process for DEP cross-over frequency (f_{co}) and cell radius (r_{cell}) data for three methods of measuring DEP-induced cell mobility.

To use the ensemble average method, we assumed that the cell DEP property was almost invariant during 7-cycles, which is supported in our previous report [37], and that the statistical analysis would only be used within a single population (see the revised Supporting Method S1 and the revised Fig. S4).

3. Results and discussion

3.1. Measurement platform for identifying heterogeneity within an isogenic population

A brief workflow for the measurement of single-cell DEP behavior on our platform is shown in Figs. 2–4. As shown in Fig. 2, cancer cells were injected into the microfluidic chamber and moved under DEP force. Cell translocation was recorded using a microscope camera system. The microelectrode array with cell-sized circular holes in the microfluidic chamber enabled manipulation at the single cell level, so that each cell was separated and placed on an individual circular hole, and then its movement was controlled in a parallel manner [9–11,37,39]. As shown in Fig. 4A, a randomly distributed individual cell was captured on each circular hole, released from the hole, and re-captured between two holes as positive and negative DEP forces (pDEP and nDEP forces) were exploited by DEP frequency modulation. Such movement experiments were repeated for 7 cycles while tracking the same individual cells in the exact same environment. Each cell's DEP movement data, which were obtained while tracking them for 7 cycles, were used to determine the effective DEP cross-over frequency (i.e., f_{co} at DEP force ≈ 0) and radius (r) of each individual cell. The f_{co} and r datasets were then used for the stochastic examination of each individual cell, as shown in Figs. 3 and 4B. The figure summarizes how we used multiple measurements from tracking single cells to calculate an ensemble average.

The results of cellular f_{co} and r after applying the individual cell tracking method are plotted in Fig. 5A–C. MCF-7 cells (breast cancer cell line) were used to evaluate the developed platform. The dataset of cellular f_{co} and r values measured as single measurements are shown in Fig. 5. In this case, it was not necessary to track each individual cell.

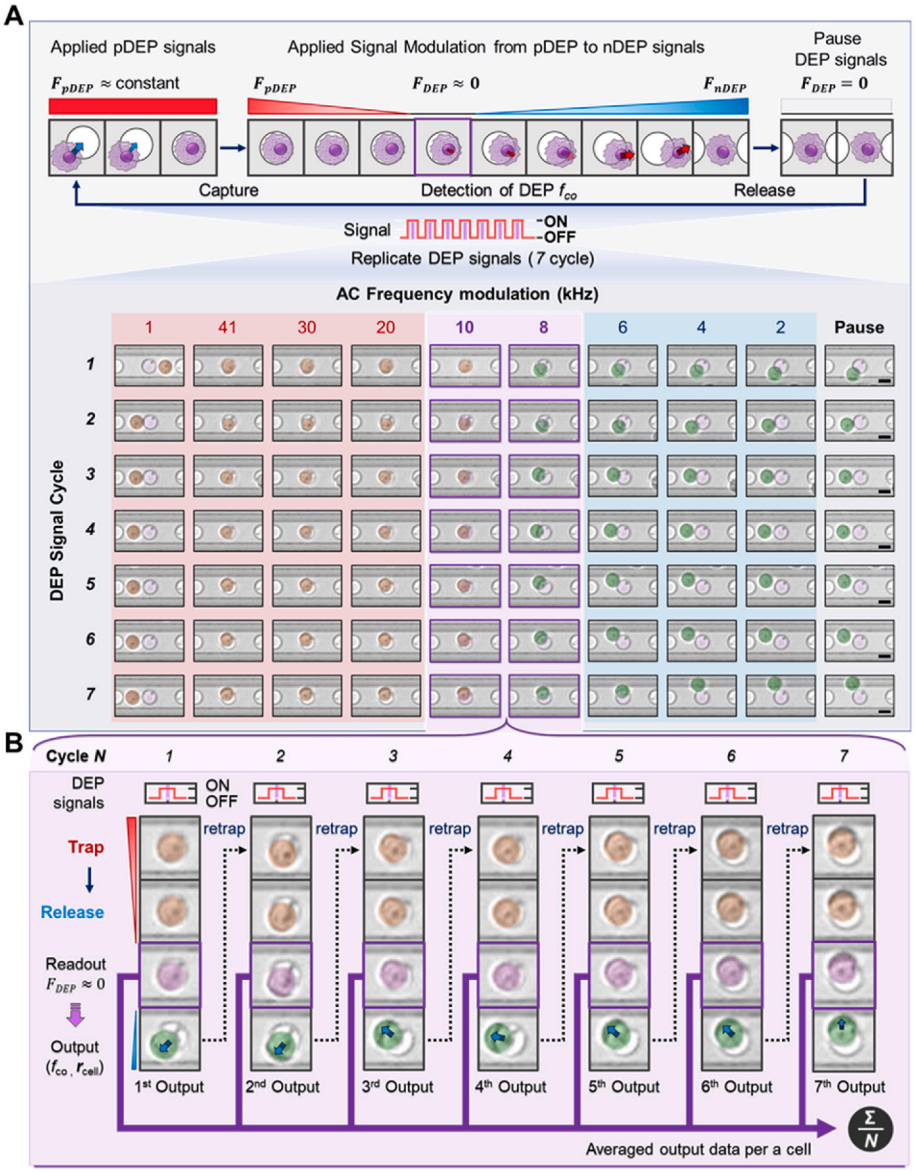

Fig. 4. Process for measuring the DEP behavior of individual cells. (**A**) Process of f_{co} determination in the sequential DEP process (see Materials and Methods for details). Time-lapse images show the translational movement of one cell during sequential AC frequency modulation (see Fig. 2 for details). Scale bar, 20 μm (**B**) Schematic representation of the per-cell DEP statistical method after obtaining ensemble f_{co} and r data by tracking each cell for 7 cycles (see Materials and Methods 2.7 and Fig. 3 for details). Σ/N represents the summation of all DEP mobility data from 7 cycles per cell divided by the number of final cycles (i.e., N = 7).

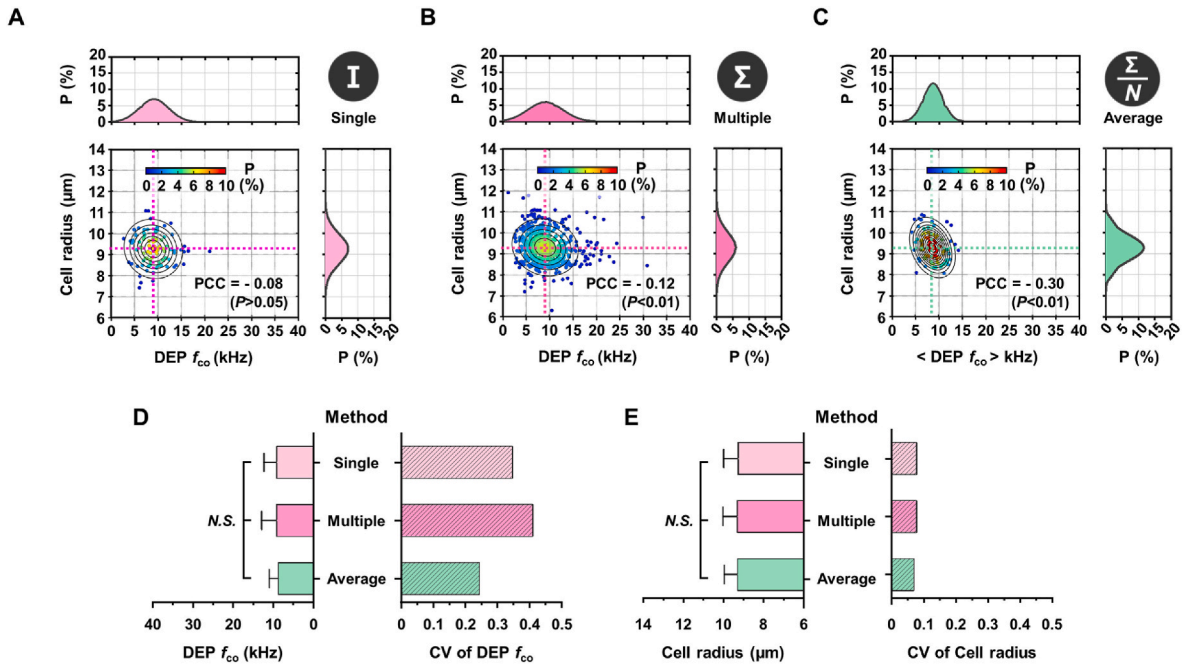

Fig. 5. Comparison of the multiple measurement–based statistical approaches used in this study to determine DEP cell mobility. (**A**) Representative scatterplot of cell radius versus cell f_{co} from a single measurement of untreated MCF-7 cells without individual cell tracking. (**B**) Representative scatterplot of cell radius versus cell f_{co} from multiple measurements (7 cycles) of untreated MCF-7 cells. (**C**) Representative scatterplot of cell radius versus cell f_{co} from averaging multiple measurements from individual untreated cells using the individual cell tracking and labeling process. (**D** and **E**) The developed methods for assessing cell f_{co} and cell r in an untreated cell population. Each left panel is the mean and standard deviation of f_{co} and r using the three developed methods. The right panel is the coefficient of variation (CV) for each method. One-way repeated ANOVA and Bonferroni's multiple comparisons of the examined cells were used to statistically compare the methods (no significant differences at $P > 0.05$ were found in any of the comparisons). All color maps correspond to the density probability of each sample. PCC is the abbreviation for the Pearson correlation coefficient, which was applied to determine the size-dependent relationship between cell r and f_{co}. The raw data are presented in Fig. S1. A total of 96 cells were used to examine this approach. The result of independent repetition experiment is described in Fig. S14.

Fig. 5B represents multiple measurements (7 cycles) from each individual cell for the whole dataset of cellular f_{co} and r values. The ensemble average dataset was produced using multiple measurements from each individual cell and the stochastic approach described in Fig. 4B is presented in Fig. 5C. The reliability and precision of the three different datasets are shown in Fig. 5D and E. The mean r and f_{co} values obtained from whole population are almost identical in the three datasets (left bars in Fig. 5D and E) and similar to the values reported in the literature [11,40–45], as we expected (Fig. S2). However, the CV of each dataset, which represents the quality of a dataset measured using a particular assay system [46], decreased dramatically when using the stochastic approach with the ensemble average extracted from multiple measurements for each individual cell. The right bars in Fig. 5D and E shows a relative improvement of f_{co} and r_{cell} in $CV_{average}$ of 15 %–40 % than $CV_{multiple}$, respectively. Therefore, our platform effectively reduces the measurement instrumentation and random noise while providing more precise and reliable ensemble averages calculated from multiple measurements for each individual cell.

Our proposed method, called the ensemble average method, effectively reduces the width of the two-dimensional cell distribution using the DEP parameters f_{co} and r_{cell} compared to the single and multiple methods. This allows for better discrimination of heterogeneous samples containing multiple subpopulations. The key factor behind this difference lies in our per-cell DEP statistical approach. First, the fundamental difference in the DEP parameters obtained from single and multiple measurements is due to the amount of data. Typically, the coefficient of variation (CV) value in repeated experiments on the same sample (cells in our case) should decrease as the number of replicates increases. This is because replicates help to reduce the variability of the data [47]. However, we did not observe this trend in our experiment when the data were not sorted by individual cells. On the other hand, the main difference between the multiple and ensemble averaging methods lies in the averaging procedure and how the data obtained for each cell are treated. In both the multiple measurement method and the ensemble average method, we used the same number of cells to calculate the CV parameter. To investigate the difference in CV between the three measurement methods, we also considered the number of experimental replicates. Fig. S3 shows the distributions of CVs for the replicate cycles in the three developed methods. Contrary to our expectations, we observed a slight increase (without MβCD) or decrease (with MβCD) in the CV values for both single and multiple measurement methods as the number of cycles increased. Although our experimental conditions, such as the applied electric field strength and the low-conductivity medium, are not critical for cell viability, with a survival rate of approximately 90 % in the trypan blue test before and after the DEP experiment, it appears that cells in these environments adapt to survive during the experiments. This adaptation likely influences our DEP f_{co} and r_{cell} parameters. However, in the ensemble average method, the CV decreased as a function of the DEP signal cycle. By fitting the data to an exponential equation ($y = y_0 + A \times EXP(R_0 \times x)$, we identified the saturation of the CV trend compared to the saturation value (i.e., y_0), as shown by the gray dashed line and the short dashed line in Fig. S3. This difference can be attributed to the process by which the effect of outliers is reduced through averaging data from multiple measurements of the same cells, thereby representing the variation of the time-averaged cell data. In summary, the observed instability in our platform contributes to these findings, rather than a dynamically variable property of the cell. We believed that the improvement in CV was due to a difference in data preprocessing from the statistical procedure of averaging all cell data acquired over all iterations. We have demonstrated that the concept of this approach is also feasible for cellular DEP applications in this work.

3.2. Ability to distinguish cellular subpopulations in an artificial cell mixture

We next evaluated the discrimination performance of the developed platform using an artificial 1:1 cell mixture of untreated and MβCD-treated cells. We used MβCD because it is known to make the membrane morphology smoother by depleting cholesterol [11,48], which implies that MβCD treatment could affect cell dielectric properties. We examined the change in cellular f_{co} in the MβCD-treated cells by applying the ensemble average method, as shown in Fig. S4. Fig. 6A–C presents the density scattering plots for the prepared cell mixture. The plots were made from the single measurement dataset, multiple measurements of the whole dataset, and multiple measurement ensemble average dataset, respectively. The data were classified using the unsupervised GMM clustering technique [49–51] under an assumed ideal condition (i.e., the existence of two subpopulations with a 1:1 ratio). The scatterplots clearly show that the ability to distinguish the two subpopulations depended on the dataset and was best with the ensemble average dataset (Fig. 6A–C).

For a more quantified comparison of the three different approaches, we evaluated a cell occupancy among classified samples as shown in Fig. 6D using the scatter plot results. In comparison to the ideal percentage in Fig. 6D, the percentages of untreated and MβCD-treated cells were 31 % and 36 %, respectively, and undecidable/indeterminable cells were 33 % in the plot made of a single measurement dataset. The plot made of multiple measurements of the whole dataset showed 37 % (untreated cells), 55 % (MβCD-treated cells) and 8 % (undecidable/indeterminable cells). The plot made of multiple measurement ensemble average datasets was the same as the true value (i.e., percentage of untreated and MβCD-treated cells were both 50 %). This shows that it is difficult to distinguish two subpopulations in cell mixture by the single measurement method or the whole data with multiple measurements method. On the other hand, the multiple measurement ensemble average data method showed complete discrimination of the mixed cells. Taken together, the reliability and selectivity of classification using the developed platform is capable of being applicable for distinguishing two different subpopulations within an isogenic cell population using our statistical approaches. The ensemble average approach combined with multiple measurements tracking each individual cell and GMM technique can be used to analyze different subpopulation groups such as untreated and drug-treated cell groups in the isogenic cell population.

In this article, we could not utilize the cell staining technique during DEP experiments because our DEP platform was equipped with brightfield microscopy instead of fluorescence microscopy. However, we were able to observe a noticeable difference in morphology between the untreated cell population and the MβCD-treated cell population when the cells detached from their culture dish due to cholesterol depletion by MβCD agents, as shown in Fig. S6. Although the distinct visual difference between the two groups was not clearly observed in the DEP chip platform after the exchange of DEP buffer, we are sure that the cells in the two groups had different roughness on their plasma membrane, characterized by folds, ruffles, and microvilli. This was based on our DEP crossover frequency results, which were based on the theory between f_{co} and the smooth cell plasma membrane [32] and previous impedance analysis [48]. In addition, we assessed the quality and quantity of the separated populations using three different methods, considering the duration of MβCD agent treatment as shown in Fig. S8. Among the three methods, the average method demonstrated the most effective discrimination between the two groups in the 1:1 mixed sample (Fig. S8E). Additionally, the trend of the f_{co} value in the separated population using the average method closely matched the results obtained from independent MβCD agent treatment time experiments (Fig. S8F). However, we acknowledge the limitation of our study in that we were unable to confirm our data with another instrument, although it seems plausible given the circumstances and our results. We will plan to address this limitation in future investigations once we have access to an additional analytical instrument.

3.3. Ability to distinguish cellular subpopulations during recovery period after MβCD treatment

To demonstrate the ability of our developed platform to distinguish cellular subpopulations in drug-induced conditions in which the true ratio of each subpopulation is unknown, we treated MCF-7 cells with MβCD for 2 h and then removed the MβCD. The cells, whose membranes were altered in response to MβCD, were allowed to recover for 24 h, and then the DEP response (cellular f_{co} and radius (r)) was analyzed. Fig. 7A–C shows the f_{co} and r values obtained from the recovered cells using the single measurement method, multiple measurement of the whole dataset method, and the multiple measurement ensemble average method, respectively. The DEP f_{co} level of the cell population returned to normal levels over time. This tendency seems to be due to the cells' self-recovery ability, as reported in a previous study [48]. Interestingly, the DEP f_{co} data had a multimodal scattering distribution, rather than a unimodal distribution, in the plots made from multiple measurements of the whole dataset and the multiple measurement ensemble average dataset, implying that two distinct cell populations existed in the

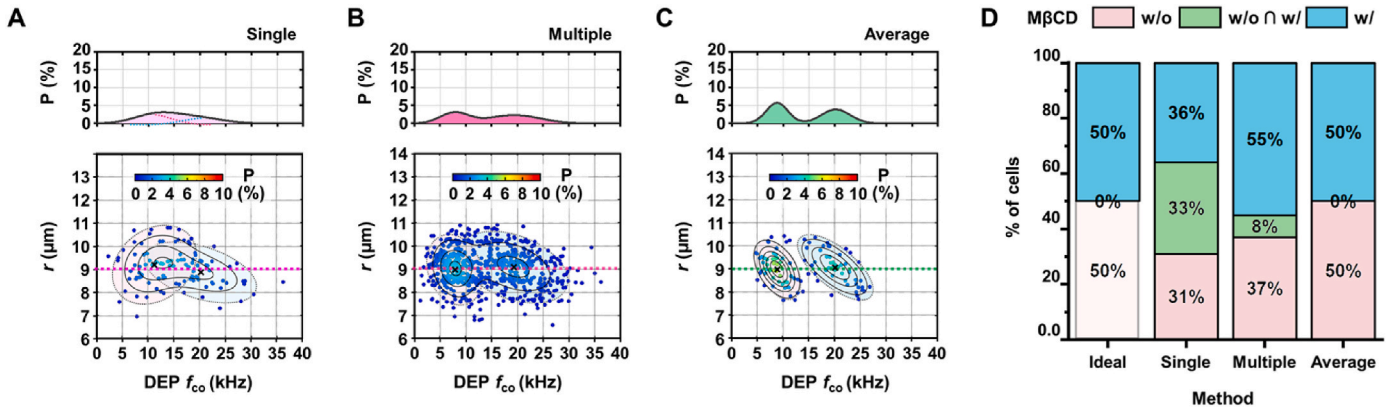

Fig. 6. Comparison of the multiple measurement–based statistics approaches for discriminating between subpopulations in a 1:1 mixture of untreated cells and MβCD-treated cells. (A–C) Representative density scatterplot of cell f_{co} versus cell radius for identical cell samples using a single measurement (A), multiple measurements (B), and ensemble averaging statistics per individual cell (C). (D) Cell occupancy among the classified samples (A–C). Each dot denotes the radius and f_{co} data of individual cells, and dot color represents the density probability for the given cells. A total of 104 cells were used to examine this approach. The result of independent repetition experiment is described in Figs. S7 and S15.

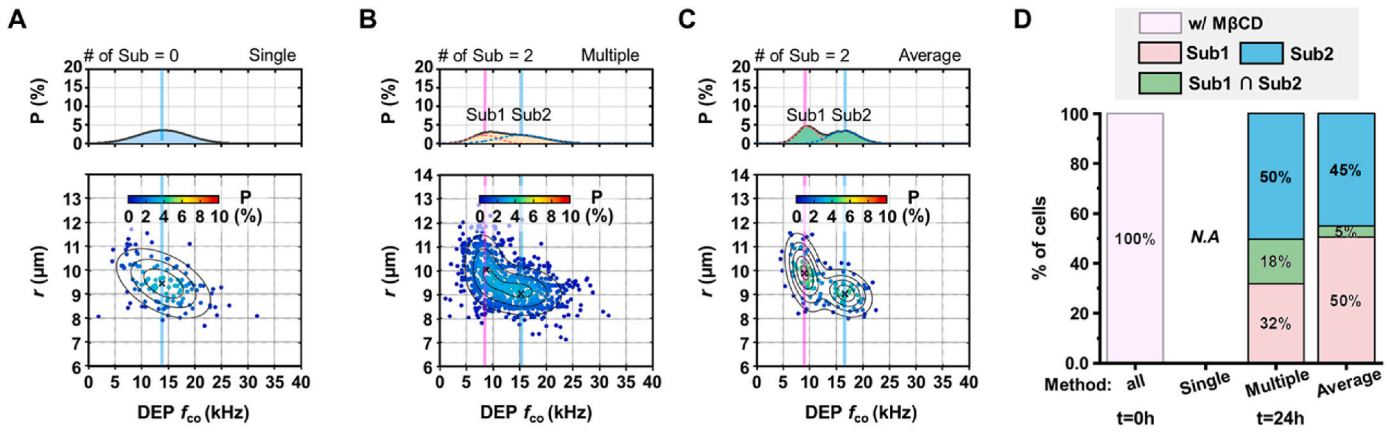

Fig. 7. Comparison of the multiple measurement–based statistical approaches for assessing cell heterogeneity during cell recovery. (**A–C**) Representative density scatterplots of cell f_{co} versus cell radius for identical cell samples using a single measurement (A), which does not distinguish cellular subpopulations, multiple measurements (B), and ensemble averaging statistics for individual cells (C), which do distinguish cellular subpopulations after 24 h in fresh serum-free Dulbecco's modified Eagle's medium buffer following MβCD treatment. The magenta and blue lines are the mean f_{co} for the cell population without and with MβCD treatment, respectively (see Fig. S8 for the mean f_{co} with and without MβCD treatment). (**D**) Cell occupancy among the classified samples with respect to the Bayesian information criterion value for each method (A–C) (see Fig. S7). A total of 114 cells were used to examine this approach. The result of independent repetition experiment is described in Figs. S16 and S17

recovered cells. We first evaluated the preference level of the cell subpopulations using the GMM model. Optimized estimations using the Bayesian information criterion, which is generally used to assess multimodal distribution status (Fig. S5) [52,53], show the existence of only one subpopulation in the plot made from the single measurement dataset and two different subpopulations in the plots made from both the multiple measurements of the whole dataset method and the multiple measurement ensemble average dataset method (Fig. 7A–C). To clarify those differences, we evaluated cell occupancy among the classified samples using scatterplots. As shown in Fig. 7D, the recovered cells could not be divided into any subpopulations in the plot made from the single measurement dataset. On the other hand, in the plots made from multiple measurements of the whole dataset, the percentages of the two distinct subpopulations were 50 % and 32 %, respectively, and with 18 % of the cells deemed indeterminable. When the data obtained from the multiple measurement ensemble average method were used, the percentages of the two distinct subpopulations were 45 % and 50 %, respectively, with only 5 % of the cells deemed indeterminable, showing that the subpopulations were best distinguished by the multiple measurement ensemble average method. In the plots made from the multiple measurement ensemble average dataset, the average f_{co} value for one population is close to that of untreated cells (magenta lines in Fig. 7A–C), implying that this subpopulation had recovered almost completely, and the average f_{co} value of the other population seems to be close to that of cells treated with MβCD for 1.5 h, suggesting that this subpopulation was partially restored (blue lines in Fig. 7A–C).

Those results indicate that two different subpopulations, which originated from an MβCD-treated isogenic cell population with 20 kHz as the mean f_{co} value, can be quantitatively classified by the ensemble average stochastic approach in combination with multiple measurement data obtained with the developed measurement platform. Subpopulation 1 (Sub1), with a lower f_{co} than the other subpopulation, is similar to the f_{co} distribution of untreated cell samples, with no statistical significance ($P > 0.05$) between them in a two-sample *t*-test. This indicates that Sub1 has almost recovered and has normal DEP properties. The other subpopulation (Sub2) shows a statistically significant correlation with the MβCD-treated cell sample ($P < 0.01$), indicating that Sub2 is still recovering from its drug-induced alteration. The DEP property of the Sub2 population was similar to the DEP property of cells treated with MβCD for 1.5 h (Fig. S11). Further investigation is needed to compare the cellular properties of the Sub2 population with those of cells treated with MβCD for 1.5 h. However, the classification accuracy was guaranteed through the consistency of the results obtained from the mixed sample of treated and untreated cells by the ensemble average approach (Figs. S12 and S13). Those results show the superior performance of the ensemble average approach over the others tested. In DEP cell manipulation, a main focus is to maintain cell viability before and after experiments in a low ionic strength buffer. In our experiment, we used the trypan blue technique to assess cell viability for 30 min after DEP, resulting in approximately 90 % viability. The conductivity of the DEP medium was 0.006 S/m under our conditions, significantly lower than that of the native cell medium, which has a conductivity over 1.5 S/m. The low conductivity of the cells increases their dielectric contrast with the surrounding media, allowing them to be effectively manipulated with DEP force. In many DEP applications, the DEP buffer is typically composed of sucrose and D-glucose to produce a low conductivity with an isotonic osmolarity similar to the native medium [9,10,37,54,55]. Unfortunately, previous studies using an isotonic sucrose/dextrose buffer (DEP buffer) for DEP manipulation have reported poor cell viability [54,56]. Moreover, the strong electric field such as 10 $V_{p\text{-}p}$ can induce cell death by altering the plasma membrane permeability when the electric potential exceeds the cell membrane potential. To enhance cell viability, we prepared a DEP buffer supplemented with BSA and PBS solutions, which have been reported to increase cell viability [9,10,37]. Additionally, we utilized an electrode design that utilizes low voltage (2 $V_{p\text{-}p}$) for the manipulation of various living cell movements. Finally, we took into account the resting duration after one cycle in AC electric signal conditions. Unfortunately, we still cannot exclude the possibility of intracellular changes including metabolism and cytoplasmic conductivity due to cell ion leakage. However, because we observed the uniformity of both cell viability, cell size, and DEP crossover frequency, which is mainly affected by the morphology of the plasma membrane, during our experiments, we believe that the impact of the unknown variable from cell internal changes will be negligible in our experiments. We will be further investigating this issue with the help of a drug for the control of the cell membrane channel. Taking our results together, we conclude that the ensemble average stochastic approach combined with multiple measurement data obtained by the developed platform can identify cellular subpopulations in recovering cell populations that are difficult to assess using bulk measurements such as electric cell substrate impedance sensing.

4. Conclusion

We developed a novel method to distinguish cellular subpopulations using an easy-to-implement and generalizable label-free platform that measures the DEP cross-over frequency (f_{co}) and cellular radius (r) of individual cells, and we decreased measurement noise by using ensemble average statistics. To verify the developed method, we first measured the f_{co} and r of untreated MCF-7 cell samples using three different methods: single measurements, multiple measurements of the whole sample for 7 cycles (tracking individual cells), and ensemble averaging of multiple measurements from each cell with the stochastic approach. A comparison of the results obtained from the three different methods shows that the ensemble average with the stochastic approach provided the best performance by reducing instrument and random noise, which allowed it to obtain more precise and reliable results. Next, we tested its ability to identify cellular subpopulations within a cell mixture by artificially mixing untreated cells and MβCD-treated cells in a 1:1 ratio. The ensemble average approach divided the untreated cells from the MβCD-treated cells, returning the correct percentage of untreated and MβCD-treated cells (50 %:50 %). Lastly, we successfully discriminated a cellular subpopulation that was recovering from MβCD-treatment based on the measured f_{co}. While the cells were recovering, we identified Sub1, with an f_{co} in good agreement with that of the untreated cell sample, and Sub2, with an f_{co} that differed from that of MβCD-treated cells. These results indicate that those subpopulations exist within the isogenic cell population during the recovery process. Specifically, Sub1 had almost recovered and showed normal DEP properties, and Sub2 was still recovering from its drug-induced alterations. In conclusion, our platform used with the ensemble average stochastic approach can identify cellular subpopulations generated by intracellular changes. Our results here suggest that our platform, which is based on an improved DEP technique, is a reliable and powerful tool for distinguishing and characterizing subpopulations generated by intracellular changes and that it opens a new avenue for next-generation multiplexed *in vitro* cell assays using measurements of dielectric cell properties.

CRediT authorship contribution statement

Seungyeop Choi: Conceptualization, Data curation, Formal analysis, Methodology, Validation, Writing – original draft, Writing – review & editing, Investigation. **Sung-Hun Woo:** Formal analysis, Investigation, Methodology, Validation, Writing – original draft, Writing – review & editing. **Insu Park:** Formal analysis, Investigation, Validation, Visualization, Writing – original draft, Writing – review & editing. **Sena Lee:** Data curation, Software, Validation. **Kang In Yeo:** Formal analysis, Investigation. **Sang Hyun Lee:** Formal analysis, Investigation. **Sei Young Lee:** Writing – review & editing, Validation. **Sejung Yang:** Software, Validation, Writing – review & editing. **Gyudo Lee:** Writing – review & editing, Validation. **Woo-Jin Chang:** Writing – review & editing, Validation. **Rashid Bashir:** Writing – review & editing, Validation. **Yoon Suk Kim:** Conceptualization, Supervision, Validation, Writing – original draft, Writing – review & editing. **Sang Woo Lee:** Conceptualization, Funding acquisition, Methodology, Supervision, Validation, Writing – original draft, Writing – review & editing.

Declaration of competing interest

The authors declare that they have no known competing financial interests or personal relationships that could have appeared to influence the work reported in this paper.

Acknowledgments

This work was supported by National Research Foundation of Korea (NRF) grants funded by the Korean government (NRF-2021R1F1A1046496, and NRF-2021R1A6A3A01086768).

Appendix A. Supplementary data

Supplementary data to this article can be found online at https://doi.org/10.1016/j.compbiomed.2024.108011.

References

[1] F.S.O. Fritzsch, C. Dusny, O. Frick, A. Schmid, Single-cell analysis in biotechnology, systems Biology, and biocatalysis, Annu. Rev. Chem. Biomol. Eng. 3 (2012) 129–155.
[2] B. Elowitz Michael, J. Levine Arnold, D. Siggia Eric, S. Swain Peter, Stochastic gene expression in a single cell, Science 297 (2002) 1183–1186.
[3] L.S. Weinberger, J.C. Burnett, J.E. Toettcher, A.P. Arkin, D.V. Schaffer, Stochastic gene expression in a lentiviral positive-feedback loop: HIV-1 tat fluctuations drive phenotypic diversity, Cell 122 (2005) 169–182.
[4] S.V. Avery, Microbial cell individuality and the underlying sources of heterogeneity, Nat. Rev. Microbiol. 4 (2006) 577–587.
[5] A. Brock, H. Chang, S. Huang, Non-genetic heterogeneity — a mutation-independent driving force for the somatic evolution of tumours, Nat. Rev. Genet. 10 (2009) 336–342.
[6] Piyush B. Gupta, Christine M. Fillmore, G. Jiang, Sagi D. Shapira, K. Tao, C. Kuperwasser, Eric S. Lander, Stochastic state transitions give rise to phenotypic equilibrium in populations of cancer cells, Cell 146 (2011) 633–644.
[7] C.C. Bell, O. Gilan, Principles and mechanisms of non-genetic resistance in cancer, Brit. J. Cancer 122 (2020) 465–472.
[8] E. Eriksson, K. Sott, F. Lundqvist, M. Sveningsson, J. Scrimgeour, D. Hanstorp, M. Goksör, A. Granéli, A microfluidic device for reversible environmental changes around single cells using optical tweezers for cell selection and positioning, Lab Chip 10 (2010) 617–625.
[9] I.S. Park, J. Lee, G. Lee, K. Nam, T. Lee, W.-J. Chang, H. Kim, S.-Y. Lee, J. Seo, D. S. Yoon, S.W. Lee, Real-time analysis of cellular response to small-molecule drugs within a microfluidic dielectrophoresis device, Anal. Chem. 87 (2015) 5914–5920.
[10] S. Choi, K. Ko, J. Lim, S. Kim, S.-H. Woo, Y. Kim, J. Key, S. Lee, I. Park, S. Lee, Non-linear cellular dielectrophoretic behavior characterization using dielectrophoretic tweezers-based force spectroscopy inside a microfluidic device, Sensors 18 (2018) 3543.
[11] I. Park, J.W. Lim, S.H. Kim, S. Choi, K.H. Ko, M.G. Son, W.-J. Chang, Y.R. Yoon, S. Yang, J. Key, Y.S. Kim, K. Eom, R. Bashir, S.Y. Lee, S.W. Lee, Variable membrane dielectric polarization characteristic in individual live cells, J. Phys. Chem. Lett. 11 (2020) 7197–7203.
[12] J.H. Koschwanez, R.H. Carlson, D.R. Meldrum, Easily fabricated magnetic traps for single-cell applications, Rev. Sci. Instrum. 78 (2007) 044301.
[13] M. Evander, L. Johansson, T. Lilliehorn, J. Piskur, M. Lindvall, S. Johansson, M. Almqvist, T. Laurell, J. Nilsson, Noninvasive acoustic cell trapping in a microfluidic perfusion system for online bioassays, Anal. Chem. 79 (2007) 2984–2991.
[14] J.S. Jeong, J.W. Lee, C.Y. Lee, S.Y. Teh, A. Lee, K.K. Shung, Particle manipulation in a microfluidic channel using acoustic trap, Biomed, Microdevices 13 (2011) 779–788.
[15] M. Tanyeri, M. Ranka, N. Sittipolkul, C.M. Schroeder, A microfluidic-based hydrodynamic trap: design and implementation, Lab Chip 11 (2011) 1786–1794.
[16] D. Gao, F. Jin, M. Zhou, Y. Jiang, Recent advances in single cell manipulation and biochemical analysis on microfluidics, Analyst 144 (2019) 766–781.
[17] G.R. Sant, K.B. Knopf, D.M. Albala, Live-single-cell phenotypic cancer biomarkers-future role in precision oncology? npj Precis. Oncol. 1 (2017) 21.
[18] N.G. Durmus, H.C. Tekin, S. Guven, K. Sridhar, A. Arslan Yildiz, G. Calibasi, I. Ghiran, R.W. Davis, L.M. Steinmetz, U. Demirci, Magnetic levitation of single cells, Proc. Natl. Acad. Sci. U.S.A. 112 (2015) E3661.
[19] D.R. Gossett, W.M. Weaver, A.J. Mach, S.C. Hur, H.T.K. Tse, W. Lee, H. Amini, D. Di Carlo, Label-free cell separation and sorting in microfluidic systems, Anal. Bioanal. Chem. 397 (2010) 3249–3267.
[20] Y. Qiang, J. Liu, M. Dao, S. Suresh, E. Du, Mechanical fatigue of human red blood cells, Proc. Natl. Acad. Sci. U.S.A. 116 (2019) 19828.
[21] J.H. Kang, T.P. Miettinen, L. Chen, S. Olcum, G. Katsikis, P.S. Doyle, S.R. Manalis, Noninvasive monitoring of single-cell mechanics by acoustic scattering, Nat. Methods 16 (2019) 263–269.
[22] J.H. Kang, G. Katsikis, Z. Li, K.M. Sapp, M.A. Stockslager, D. Lim, M.G. Vander Heiden, M.B. Yaffe, S.R. Manalis, T.P. Miettinen, Monitoring and modeling of lymphocytic leukemia cell bioenergetics reveals decreased ATP synthesis during cell division, Nat. Commun. 11 (2020) 4983.
[23] S. Huda, B. Weigelin, K. Wolf, K.V. Tretiakov, K. Polev, G. Wilk, M. Iwasa, F. S. Emami, J.W. Narojczyk, M. Banaszak, S. Soh, D. Pilans, A. Vahid, M. Makurath, P. Friedl, G.G. Borisy, K. Kandere-Grzybowska, B.A. Grzybowski, Lévy-like movement patterns of metastatic cancer cells revealed in microfabricated systems and implicated in vivo, Nat. Commun. 9 (2018) 4539.
[24] C. Metzner, C. Mark, J. Steinwachs, L. Lautscham, F. Stadler, B. Fabry, Superstatistical analysis and modelling of heterogeneous random walks, Nat. Commun. 6 (2015) 7516.
[25] K. Dholakia, B.W. Drinkwater, M. Ritsch-Marte, Comparing acoustic and optical forces for biomedical research, Nat. Rev. Phys. 2 (2020) 480–491.

[26] T. Lannin, W.-W. Su, C. Gruber, I. Cardle, C. Huang, F. Thege, B. Kirby, Automated electrorotation shows electrokinetic separation of pancreatic cancer cells is robust to acquired chemotherapy resistance, serum starvation, and EMT, Biomicrofluidics 10 (2016) 064109.
[27] H.-W. Su, J.L. Prieto, J. Voldman, Rapid dielectrophoretic characterization of single cells using the dielectrophoretic spring, Lab Chip 13 (2013) 4109–4117.
[28] C. Honrado, N. Michel, J.H. Moore, A. Salahi, V. Porterfield, M.J. McConnell, N. S. Swami, Label-free quantification of cell cycle synchronicity of human neural progenitor cells based on electrophysiology phenotypes, ACS Sens. 6 (2020) 156–165.
[29] E.A. Henslee, P. Crosby, S.J. Kitcatt, J.S.W. Parry, A. Bernardini, R.G. Abdallat, G. Braun, H.O. Fatoyinbo, E.J. Harrison, R.S. Edgar, K.F. Hoettges, A.B. Reddy, R. I. Jabr, M. von Schantz, J.S. O'Neill, F.H. Labeed, Rhythmic potassium transport regulates the circadian clock in human red blood cells, Nat. Commun. 8 (2017) 1978.
[30] A. Schmid, H. Kortmann, P.S. Dittrich, L.M. Blank, Chemical and biological single cell analysis, Curr. Opin. Biotechnol. 21 (2010) 12–20.
[31] Y. Zhang, J. Zhao, H. Yu, P. Li, W. Liang, Z. Liu, G.-B. Lee, L. Liu, W.J. Li, Z. Wang, Detection and isolation of free cancer cells from ascites and peritoneal lavages using optically induced electrokinetics (OEK), Sci. Adv. 6 (2020) eaba9628.
[32] I. Turcan, M.A. Olariu, Dielectrophoretic manipulation of cancer cells and their electrical characterization, ACS Comb. Sci. 22 (2020) 554–578.
[33] J. Lu, C.A. Barrios, A.R. Dickson, J.L. Nourse, A.P. Lee, L.A. Flanagan, Advancing practical usage of microtechnology: a study of the functional consequences of dielectrophoresis on neural stem cells, Integr. Biol. 4 (2012) 1223–1236.
[34] J.L. Prieto, J. Lu, J.L. Nourse, L.A. Flanagan, A.P. Lee, Frequency discretization in dielectrophoretic assisted cell sorting arrays to isolate neural cells, Lab Chip 12 (2012) 2182–2189.
[35] J. Yang, Y. Huang, X. Wang, X.-B. Wang, F.F. Becker, P.R.C. Gascoyne, Dielectric properties of human leukocyte subpopulations determined by electrorotation as a cell separation criterion, Biophys. J. 76 (1999) 3307–3314.
[36] E.A. Henslee, Review: dielectrophoresis in cell characterization, Electrophoresis 41 (2020) 1915–1930.
[37] S. Choi, H. Lee, S. Lee, I. Park, Y.S. Kim, J. Key, S.Y. Lee, S. Yang, S.W. Lee, A novel automatic segmentation and tracking method to measure cellular dielectrophoretic mobility from individual cell trajectories for high throughput assay, Comput. Methods Progr. Biomed. 195 (2020) 105662.
[38] M.H. Kim, J. Lee, K. Nam, I.S. Park, M. Son, H. Ko, S. Lee, D.S. Yoon, W.-J. Chang, S.Y. Lee, Y.R. Yoon, S.W. Lee, Automated dielectrophoretic tweezers-based force spectroscopy system in a microfluidic device, Sensors 17 (2017) 2272.
[39] R.H. Cole, S.-Y. Tang, C.A. Siltanen, P. Shahi, J.Q. Zhang, S. Poust, Z.J. Gartner, A. R. Abate, Printed droplet microfluidics for on demand dispensing of picoliter droplets and cells, Proc. Natl. Acad. Sci. U.S.A. 114 (2017) 8728.
[40] H.M. Coley, F.H. Labeed, H. Thomas, M.P. Hughes, Biophysical characterization of MDR breast cancer cell lines reveals the cytoplasm is critical in determining drug sensitivity, Biochim. Biophys. Acta Gen. Subj. 1770 (2007) 601–608.
[41] E.A. Henslee, Exploiting Clausius-Mossotti Factor to Isolate Stages of Human Breast Cancer Cells: Theory and Experiment, Virginia Tech, 2010.
[42] C. Huang, C. Liu, B. Minne, J.E. Ramirez Hernandez, T. Stakenborg, L. Lagae, Dielectrophoretic discrimination of cancer cells on a microchip, Appl. Phys. Lett. 105 (2014) 143702.
[43] W. Liang, Y. Zhao, L. Liu, Y. Wang, W.J. Li, G.-B. Lee, Determination of cell membrane capacitance and conductance via optically induced electrokinetics, Biophys. J. 113 (2017) 1531–1539.
[44] Z. Zhang, T. Zheng, R. Zhu, Characterization of single-cell biophysical properties and cell type classification using dielectrophoresis model reduction method, Sens. Actuator B-Chem. 304 (2020) 127326.
[45] Y. Feng, Z. Cheng, H. Chai, W. He, L. Huang, W. Wang, Neural network-enhanced real-time impedance flow cytometry for single-cell intrinsic characterization, Lab Chip 22 (2022) 240–249.
[46] Z. Jalilibal, A. Amiri, P. Castagliola, M.B.C. Khoo, Monitoring the coefficient of variation: a literature review, Comput. Ind. Eng. 161 (2021) 107600.
[47] N. Malo, J.A. Hanley, S. Cerquozzi, J. Pelletier, R. Nadon, Statistical practice in high-throughput screening data analysis, Nat. Biotechnol. 24 (2006) 167–175.
[48] A. Pietuch, B.R. Brückner, T. Fine, I. Mey, A. Janshoff, Elastic properties of cells in the context of confluent cell monolayers: impact of tension and surface area regulation, Soft Matter 9 (2013) 11490–11502.
[49] M.D. Slack, E.D. Martinez, L.F. Wu, S.J. Altschuler, Characterizing heterogeneous cellular responses to perturbations, Proc. Natl. Acad. Sci. U.S.A. 105 (2008) 19306.
[50] I. Prabakaran, Z. Wu, C. Lee, B. Tong, S. Steeman, G. Koo, P.J. Zhang, M. A. Guvakova, Gaussian mixture models for probabilistic classification of breast cancer, Cancer Res. 79 (2019) 3492.
[51] D. Lee, A. Jayaraman, J.S.I. Kwon, Identification of cell-to-cell heterogeneity through systems engineering approaches, AIChE J. 66 (2020) e16925.
[52] S. Chen, P.I. Imoukhuede, Single-cell receptor quantification of an in vitro coculture angiogenesis model reveals VEGFR, NRP1, Tie2, and PDGFR regulation and endothelial heterogeneity, Processes 7 (2019) 356.
[53] A. Parthasarathy, S. Romero Pinto, R.M. Lewis, W. Goedicke, D.B. Polley, Data-driven segmentation of audiometric phenotypes across a large clinical cohort, Sci. Rep. 10 (2020) 6704.
[54] S.V. Puttaswamy, S. Sivashankar, R.-J. Chen, C.-K. Chin, H.-Y. Chang, C.H. Liu, Enhanced cell viability and cell adhesion using low conductivity medium for negative dielectrophoretic cell patterning, Biotechnol. J. 5 (2010) 1005–1015.
[55] J. Cemazar, A. Ghosh, R.V. Davalos, Electrical manipulation and sorting of cells, in: W. Lee, P. Tseng, D. Di Carlo (Eds.), Microtechnology for Cell Manipulation and Sorting, Springer International Publishing, Cham, 2017, pp. 57–92.
[56] A.C. Sabuncu, A.J. Asmar, M.W. Stacey, A. Beskok, Differential dielectric responses of chondrocyte and Jurkat cells in electromanipulation buffers, Electrophoresis 36 (2015) 1499–1506.